Title
THE LIFETIME AND DECAY MODES OF NEGATIVE K MESONS

Author
Nickols, Norris A.

Publication Date
1959-09-01

UNIVERSITY OF
CALIFORNIA

Ernest O. Lawrence
Radiation Laboratory

THE LIFETIME AND DECAY MODES OF NEGATIVE K MESONS

DISCLAIMER

UCRL-8692
Physics and Mathematics
TID-4500 (15th Ed.)

UNIVERSITY OF CALIFORNIA
Lawrence Radiation Laboratory
Berkeley, California

Contract No. W-7405-eng-48

THE LIFETIME AND DECAY MODES OF NEGATIVE K MESONS

Norris A. Nickols

(Thesis)

September 1959

Printed for the U.S. Atomic Energy Commission

Printed in USA. Price $1.25. Available from the
Office of Technical Services
U. S. Department of Commerce
Washington 25, D.C.

THE LIFETIME AND DECAY MODES OF NEGATIVE K MESON

Contents

THE LIFETIME AND DECAY MODES OF NEGATIVE K MESONS

Norris A. Nickols

Lawrence Radiation Laboratory
University of California
Berkeley, California

September 1959

ABSTRACT

A large emulsion stack exposed to an enriched K^--meson beam analyzed by 180-deg magnetic bending has been used to measure the mean lifetime and decay branching ratios of K^- mesons. In a systematic study of 2582 K^- mesons, 86 events in flight with no stable prong, blob, or Auger electron were observed. Of these, 48 had one lightly ionizing secondary and 38 had no visible secondary. No τ^- were observed. Space angles were measured and momenta of secondaries were determined from their ranges or from blob-density measurements. The residual range accurately determined the K^--meson momentum at the decay point, because the 180-deg. bending provided high momentum resolution. A probability analysis was used to calculate the relative populations of the various decay modes and of nuclear interactions that simulate decays. Independent estimates of upper and lower limits to the number of decays present were made. The percent branching ratios for the various decay modes measured are as follows: $K^-_{\mu 2}$ (56.5 ± 7.3), $K^-_{\mu 3}$ (9.5 ± 4.3), $K^-_{\pi 2}$ (26.3 ± 6.6), $K^-_{\pi 3}$ (2.8 ± 2.4), K^-_{e3} (4.9 ± 3.2), τ^- (0.0 + 2.1). The K^--meson mean lifetime is $1.25\ ^{+0.22}_{-0.17} \times 10^{-8}$ sec.

INTRODUCTION

In recent years the development of beams of artificially produced K mesons at the Bevatron of The Lawrence Radiation Laboratory and at the Brookhaven Cosmotron has greatly facilitated the study of these particles, which were first observed in cosmic radiation.

The lifetime and relative frequency of the various decay modes for the K^+ meson have been measured by several experimenters using emulsion[1-6] and counters.[7,8] The value for the lifetime is $(1.223 \pm 0.013) \times 10^{-8}$ sec.[9] The decay modes observed, together with the relative frequencies determined by Birge et al.[5] and by Alexander, Johnson, and O'Ceallaigh[6] are given below.

Decay Mode	Relative Frequency (%)	
	Birge et al.	Alexander, Johnson and O'Ceallaigh
$\tau^+ \rightarrow \pi^+ + \pi^+ + \pi^-$	5.56±0.41	6.77±0.45
$\tau'^+ \rightarrow \pi^+ + \pi^0 + \pi^0$	2.15±0.47	2.15±0.45
$K^+_{\mu 2} \rightarrow \mu^+ + \nu$	58.2±3.0	57.0±2.6
$K^+_{\pi 2} \rightarrow \pi^+ + \pi^0$	28.9±2.7	23.2±2.2
$K^+_{\mu 3} \rightarrow \mu^+ + \pi^0 + \nu$	2.83±0.95	5.9±1.3
$K^+_{e3} \rightarrow e^+ + \pi^0 + \nu$	3.23±1.30	5.1±1.3

If, as has been assumed, the K^+ and K^- mesons are particle and antiparticle, PCT invariance would require them to have identical lifetimes and branching ratios between the decay modes. A difference in either quantity would mean that they are not particle and antiparticle, or that the PCT theorem is violated. Although neither alternative now seems likely, at the time this investigation was started almost no experimental data existed to test these axioms of elementary particle theory. Only isolated examples of K^- meson decays had been identified and lifetime measurements had large errors.

Since that time two groups have reported more systematic studies: Eisenberg et al.[10] have made a systematic study of about 1600 K^- mesons in emulsion and found two events which they have identified as τ^-, and 38 stars in flight with one lightly ionizing secondary and no indication of an interaction, 22 of which they find analyzable. They report good examples of $K_{\mu 2}$ and $K_{\pi 2}$ modes and report relative abundances among modes exclusive of τ as

65±18%	$K_{\mu 2}$ plus K_{e3} and some $K_{\mu 3}$;
30±12%	$K_{\pi 2}$ plus some $K_{\mu 3}$, perhaps one K_{e3};
5±5%	$K_{\pi 3}$.

Their value for the lifetime is

$$T_{k-} = (1.60 \pm 0.3) \times 10^{-8} \text{ sec.}$$

Nilsson and Frisk[11] have observed 21 possible decays in a systematic study of K^- mesons and report conclusive evidence for τ^-, $K^-_{\mu 2}$, and K^-_{e3} modes as well as events consistent with $K^-_{\mu 3}$, $K^-_{\pi 2}$, and $K^-_{\pi 3}$ and the abundance ratios $\tau^-/(K^-_L + \tau^-) = 0.15$ and $K^-_{\pi 2}/K^-_{\mu 2} = 0.43$. Their lifetime value is $(1.50^{+0.45}_{-0.30}) \times 10^{-8}$ sec. Other measurements indicate a K^--meson lifetime consistent with that of the positive meson,[12-17] but it is clear that a much better knowledge of K^--meson lifetime as well as of branching ratios is needed to establish the above-mentioned identities.

The study of K^--meson decays is made much more difficult than the comparable positive meson study by the lower production of K^- mesons and the strong K^--meson-nucleon interaction. Since the K^-/K^+ production ratio is only about 0.01, K^--meson beams will be 1% as intense as similar K^+-meson beams. More serious are the complications introduced by the strong nuclear interaction of K mesons. In contrast to the K^+ meson, which decays upon coming to rest, the K^- undergoes nuclear capture so that only decays in flight are observed. These

constitute but a few percent of the total number entering a detector and are contaminated by interactions in flight which give rise to one lightly ionizing pion. The analysis of decays in flight requires, in addition to the determination of the identity of the secondary and its momentum, the determination of the K momentum and the angle between the two. Because of the short length of track observed and the momentum dispersion common in K-meson beams, the K-meson momentum is usually measurable only with large errors, and fast secondaries often leave the detector with trajectories too short to permit their identification or determination of their momentum.

For the strange-particle studies of which this work is a part an enriched beam of K^- mesons was developed. As a detector we used a stack of nuclear track emulsion, denoted 2B, large enough that some of the decay secondaries would come to rest and most would leave enough track to completely identify them. The size of this stack, 9X12X6 inches, combined with the high flux, relatively low pion contamination, and particularly the low momentum dispersion of the K-meson beam, made this study feasible.

Some of the data used in this thesis have been reported previously.[18]

BEAM DEVELOPMENT

Negative particles that leave the 73-degree target in the northwest quadrant of the Bevatron in the forward direction relative to the primary proton beam are deflected outward by the Bevatron magnetic field, and those of appropriate momentum pass through a slot in the magnet yoke. We attempted to separate K^- mesons from this "beam" by using an energy degrader and an analyzing magnet.

As a preliminary step the momentum spectrum and exit angles of these particles were determined by plotting particle trajectories representing various momenta from the target position, using the "mechanical particle." This device, a motor-driven tricycle, draws a pen over magnetic-field contours as the operator varies the angle of the front wheel to maintain the proper radius of curvature. It is an improved model of one designed and built by Rankin,[19] differing only in constructional details. The orbits showed that particles with momenta in the band 435±20 Mev/c would pass through the slot and exit radially (within 3 deg) from the Bevatron. The 90 deg deflection in the Bevatron field tends to focus particles horizontally, so that in the median plane trajectories of particles of the same momentum leave the Bevatron approximately parallel. This is coupled with a slight vertical defocus. Wire orbits through the quadrupole focusing magnet showed that essentially all this beam could be focused, and determined the current settings used.

A 180-deg focusing magnet gives, in addition to a large angular collection of particles, a momentum gradient at the detector with a point-to-point correspondence of momentum to radial position. We particularly wished to avail ourselves of this feature for the analyzing magnet, because of the assistance it would lend to the analysis of in-flight events. Special pole tips, designed to provide a field capable of deflecting 300-Mev/c particles through 180 deg on a radius of 20 inches with a 6-inch gap, were built and installed in the 40-inch Sagane magnet. The median-plane field of this magnet was mapped with a bismuth probe and rotating-coil gaussmeter so that the mechanical

particle could be used to study its focusing and bending properties. Orbits representing various momenta were plotted from several positions along the entrance edge and at different angles to select the central K-meson momentum, the detector position, and the orientation of the magnet with the beam which would give the best collection of K mesons and best rejection of pions. These orbits predicted a complete separation between the 300-Mev/c K mesons and 394-Mev/c pions. That this was not achieved was probably due to scattering in the degrader, shielding, and magnet structure, and to secondary-pion sources inside and outside the Bevatron. In the final setup wire orbits in the analyzing magnet and test plates at various positions along the beam checked the correctness of the plotted orbits, except that the central momentum at the exit of the Bevatron was found to be 427 Mev/c. This decrease was accounted for by the energy loss in the wall of the vacuum tank and possibly by a small uncertainty in our knowledge of the Bevatron field and target position.

EXPERIMENTAL ARRANGEMENT

The final arrangement used for the exposure of the 1U and 2B stacks is shown in Fig. 1: 6.2-Bev protons strike a $1/2 \times 1 \times 3.5$-inch copper flip-up target located at the 73-deg position in the northwest quadrant. Negative particles leaving the target in the forward direction relative to the primary proton beam are deflected toward the outer wall by the Bevatron magnetic field, and those with momentum in the band 435±20 Mev/c pass through a slot in the magnet yoke used as a collimator. This beam exits radially from the Bevatron and consists of 6×10^3 particles per cm^2 per 10^{10} protons on the target, with a π^-/K^- ratio of 3000/1. A quadrupole magnet focuses the beam on a polystyrene energy degrader of nominal thickness 19.4 g/cm^2, which is placed at the entrance to the analyzing magnet. Traversal of the degrader reduces the central pion momentum to 394 Mev/c and that of the K mesons to 300 Mev/c. The analyzing magnet then deflects the K mesons through approximately 180 deg and into the stack, effecting a final separation of 19 inches between the peaks of the K-meson and pion beams. At the stack position the flux is 50 K^-/cm^2 per 10^{13} protons on the target, with 800 background tracks per K meson. The background tracks, consisting of 80% muons, 10% pions, and 10% electrons, are minimum-ionizing, while the K mesons are twice minimum. The pion fraction was determined by the attenuation of the star-forming component and that of the electrons by their characteristic cascade multiplication with penetration into the stack. The muons come chiefly from the decay in flight of pions, and are not a serious hindrance to the scanning since they are noninteracting. The momentum gradient along the face of the stack is 1.6 Mev/c per cm, with a ± 2% dispersion.

The 2B stack consisted of 240 pellicles, 9×12-inches by 600μ, of Ilford G.5 emulsion, and was exposed so that the beam entered the edge of the pellicles, normal to the 12-inch side. The 1U stack, a smaller test stack of 120 pellicles, 3×6-inches by 600μ, also yielded decay information, although it was too small to permit extensive analysis.

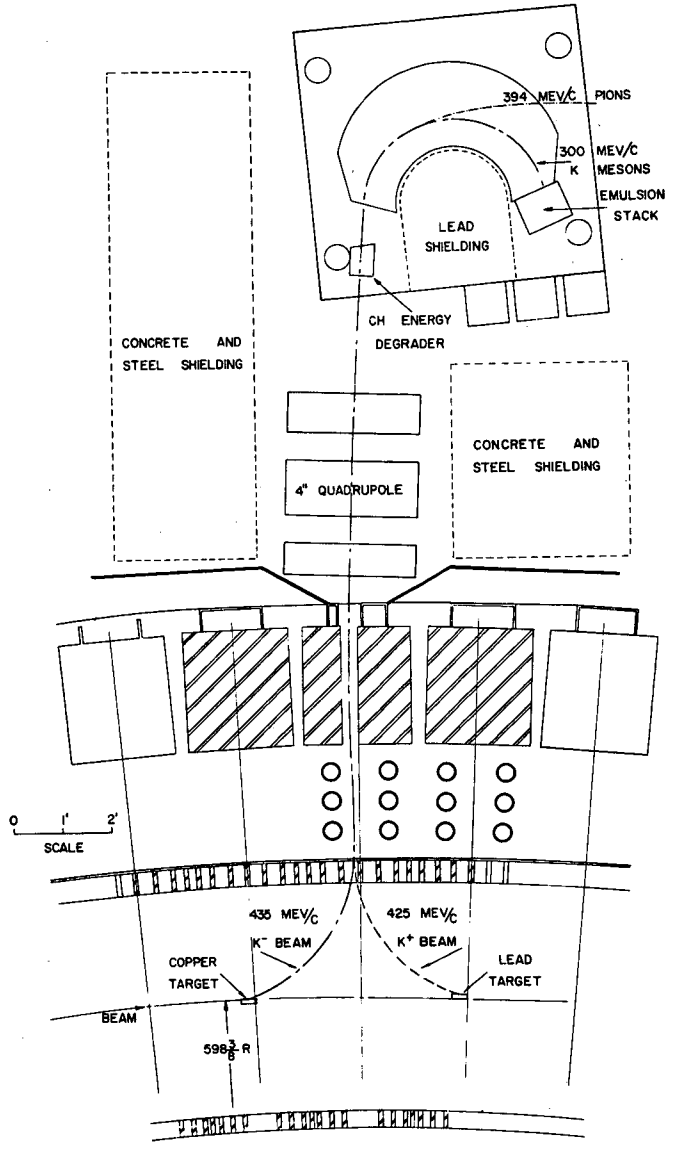

Fig. 1. Plan drawing of the experimental arrangement at the Bevatron.

Before disassembly of the stacks for processing, notches were milled in the edge opposite the entrance edge to act as fiducial marks for printing a grid on each pellicle. The grid, consisting of a two-dimensional array of numbers in 1-mm squares, is contact-printed on the bottom of each pellicle prior to mounting it on glass, to aid in the following of tracks from one pellicle to another.

SCANNING PROCEDURES

To provide an unbiased sample of K^- mesons for the various studies of strange particles for which the 2B stack was intended, "along-the-track" scanning was employed. Scanners were instructed to scan along a line 1 mm from the entrance edge of the pellicle and pick up tracks of approximately twice minimum ionization. Those tracks lying within 10 deg of the average direction of minimum-ionizing tracks in that region were followed until they decayed or interacted. The efficiency for finding true K^- mesons by using this method was better than 95%. Each event was verified by a physicist while it was in the field of the scanner's microscope, and recorded.

During the scanning of the 2 B stack we introduced a new system for recording and filing data, using 8.5X11-inch McBee keysort cards as shown in Fig. 2. A card is punched for each event, the holes across the top representing information on the initial particle and those on either side relating to secondary particles. This system proved to be of great value in cataloging events, and all previously recorded 2 B data were transferred to punched cards.

Events in flight, with one (or three) prongs and no indication of an interaction--i.e. blob, recoil, or electron--were tentatively indentified as decays. Those events with no evidence of an interaction or a prong were identified as "disappearances in flight" and subsequently re-examined for a possible minimum-ionizing secondary.

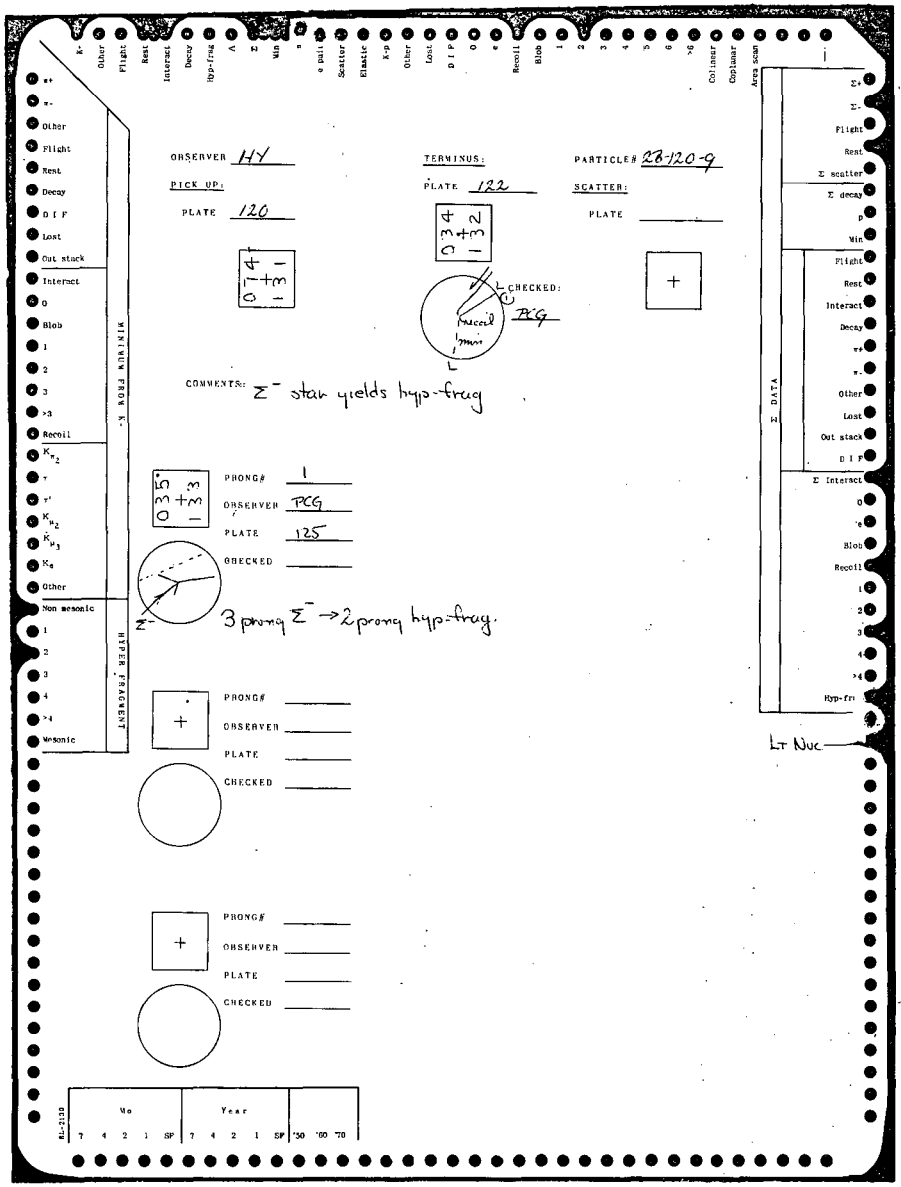

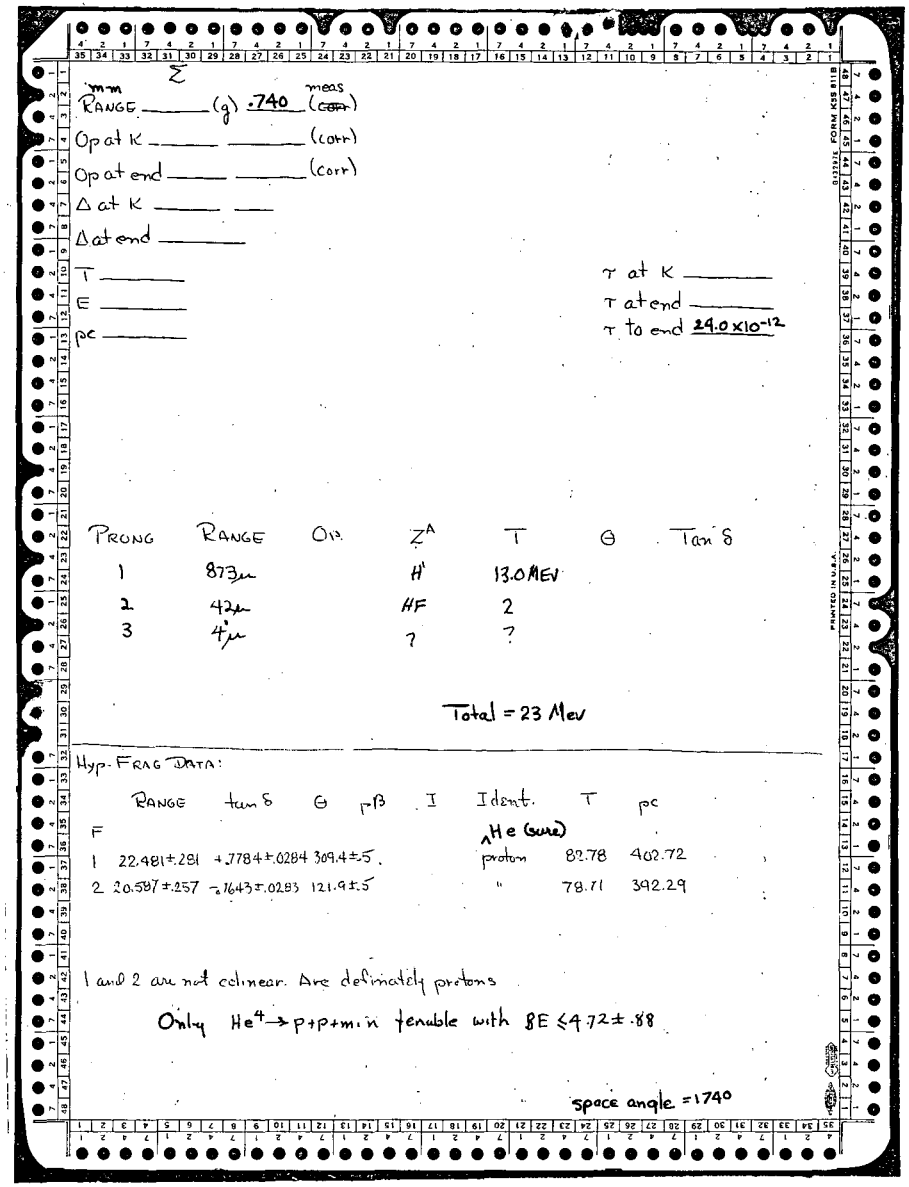

MUB-218

Fig. 2. Example of keysort card used for recording data.

MEASUREMENTS

Emulsion Density and Shrinkage Factor

Since the range-energy relations are dependent upon the emulsion density at the time of exposure it must be accurately known for precise range measurements. The density of each of six emulsion batches in the 2B stack was determined from the displacement in carbon tetrachloride of small samples cut from several pellicles. The average density was 3.815 g/cm^3, with a small variation that was not significant in this work .

Emulsion shrinks in thickness, during processing, by a factor of about two, and this shrinkage factor must be determined for accurate range and angle measurements. Although it could be arrived at, in principle, by measuring the thickness of each pellicle before and after processing, the difficulty of measuring thicknesses accurately in the darkroom necessitates a more indirect approach. The procedure used for the 2B stack was as follows. Before disassembling the stack we measured its total thickness and mass, the thickness including some air space between pellicles. After processing, the area of each pellicle was measured, and from this, the unprocessed mass, and the unprocessed emulsion density, the mean thickness before processing was calculated. The mean pellicle thickness before processing was 634.61 microns. After processing the thickness of each pellicle was measured in three places with a microscope. To correct for variations in the shrinkage factor with varying humidity, the pellicle thickness at the time a measurement is taken is compared with the original and a new shrinkage factor computed. Because of its size the 2 B stack had to be processed in four batches, each of which had its own shrinkage factor.

Mean Stopping Line

Because of the aforementioned momentum gradient and low dispersion of the beam, there is a well-defined mean stopping line for K^- mesons in the 2 B stack. This was determined graphically by plotting the interaction point of each stopping K^- meson on a graph-paper

representation of the grid, ten times actual size. These points lie along a straight line, as shown in Fig. 3. The lines on either side of the mean stopping line are standard-deviation lines which enclose 68% of the interaction points. The residual range of a decaying K meson is then the distance along the beam direction from the decay point to the mean stopping line with a standard deviation given by the distance from the mean stopping line to the standard deviation line at that point. This determines the K-meson momenta with standard deviations less than 10% for those with residual ranges greater than 5mm. Ionization measurements were used to determine the residual ranges of those which decayed within 5 mm of the mean stopping line. A program was written for the IBM 650 which derives the kinetic energy, momentum, and the velocity parameters $\beta=v/c$ and $\gamma=(1-\beta^2)^{-1/2}$ of a particle from its mass and residual range in emulsion, using the Barkas range-energy tables.[20] Errors on the quantities are computed from the errors on the range. The K^--meson ranges and momenta will be seen in columns 2 through 4 of Table I. The errors on P_k are in general much less than 10%.

Angle Measurements

The space angle between the direction of the K meson and that of its secondary was computed from the projected angle between them and from their dip angles. Thickness measurements were made on the pellicle at the time of the angle measurement to compute the shrinkage factor. The errors involved in angle measurements arise from multiple scattering of the particles, observer errors, granularity, and errors in the shrinkage factor. In this study 0.5 deg has been taken as the total error on the projected angle, and the error on the dip angle has been estimated for each case, since it varies with dip angle. Space angles near 70 deg, where the momentum of the secondary is most sensitive to the space angle, were remeasured at least once.

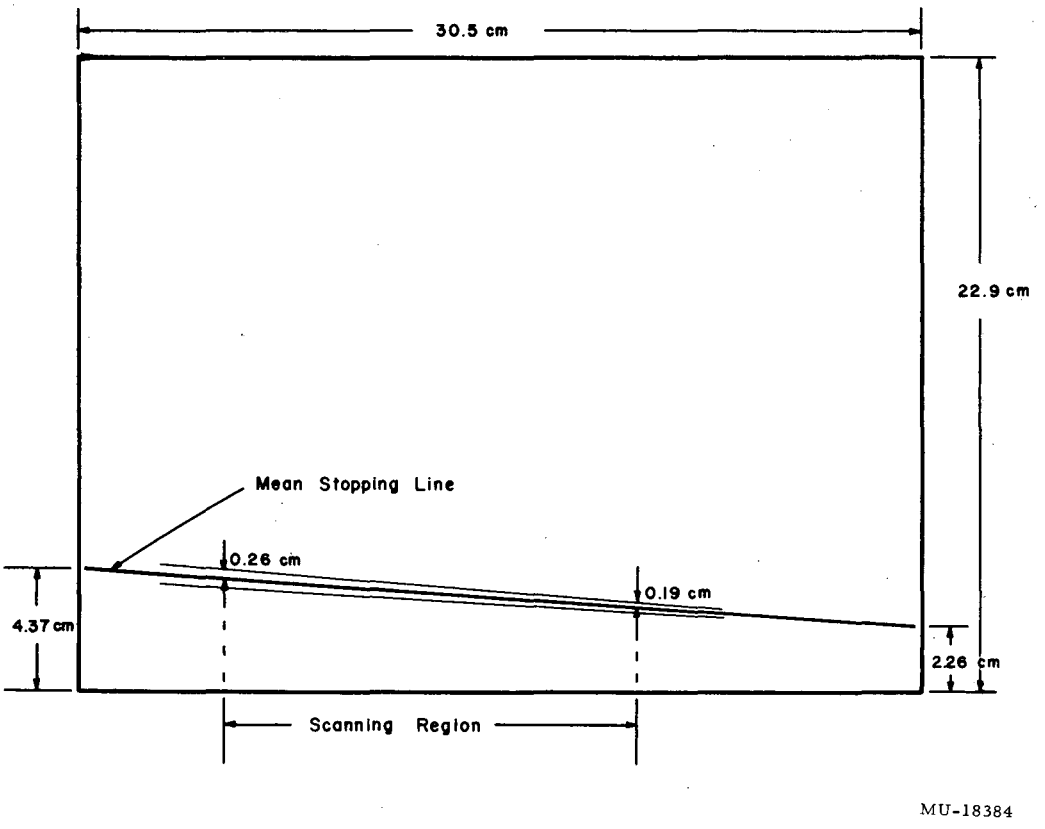

Fig. 3. Diagram indicating stopping positions for K^- mesons in pellicles.

Decay Kinematics

The kinematics of the decay of a charged particle into one charged and one neutral particle are described by the equation

$$E_1E_2 - P_1P_2 \cos\theta = C,\ C = 1/2\ (M_1^2 + M_2^2 - M_n^2),$$

where the subscripts 1 and 2 refer to the primary and the charged secondary respectively, θ is the laboratory-system angle between their directions, E is the total energy of a particle and P its momentum, and C is a function of the masses of the three particles. To aid in the analysis, curves of P_2 as a function of θ at constant P_1 were drawn for the $K_{\mu 2}$, $K_{\pi 2}$, $K_{\mu 3}$, and $K_{\pi 3}$ modes and are shown in Appendix I. For the three-body decays these curves give the maximum momentum of the secondary. A program was written for the IBM 650 which computes the space angle and its total error from the angle measurements, and from this space angle and from the K-meson momentum and the error on the K-meson momentum, it computes the secondary momentum for a given decay mode together with its total error.

Ionization Measurements

A special microscope with a motor-driven stage and an electronic data tabulator were built to aid the ionization measurements in this work. This device tabulates the blob density, density of gaps greater than a preset length, and the lacunarity (or linear transparency) on one traversal of the track. It is described more fully in Appendix II.

Secondaries that left the stack or interacted in flight were blob-counted for at least 1000 counts as near the end of their range as possible to determine their momenta at the decay point. A calibration of blob density as a function of residual range was made with stopping π mesons, and the minimum blob density in each pellicle used for counting was established by using secondaries of the identified two-body decays near their decay point. Minimum blob density varied from 14 to 19 blobs per 100 microns in the 2B stack. The blob density (in units of minimum blob density as a function of pion residual range)

is shown in Fig. 4. The maximum blob density on this curve came from measurements on stopping K mesons. Since the blob density is a function of particle velocity only and the residual range of a particle at a given velocity is proportional to its mass, residual ranges of particles other than pion are obtained from this graph by multiplying the pion residual range by the ratio of the mass to that of the pion.

The dip-angle correction for blob density was derived as follows.

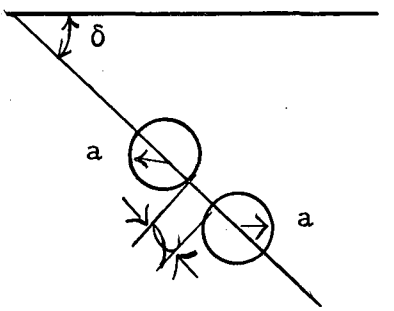

Fig. 5

Consider two spherical grains of radius a and separation ℓ in a track oriented at a dip angle δ such that they appear to just touch and would be counted as one blob. Then only gaps greater than ℓ will be observed and counted. From Fig. 5 we have

$$2a + \ell = 2a \sec \delta,$$

$$\ell = 2a (\sec \delta - 1) = D (\sec \delta - 1).$$

Barkas has derived the relation

$$H_\ell = Be^{-g\ell},$$

where B is the blob density, H_ℓ is the number of gaps greater than ℓ, and g is the grain density.[21] Therefore we will see

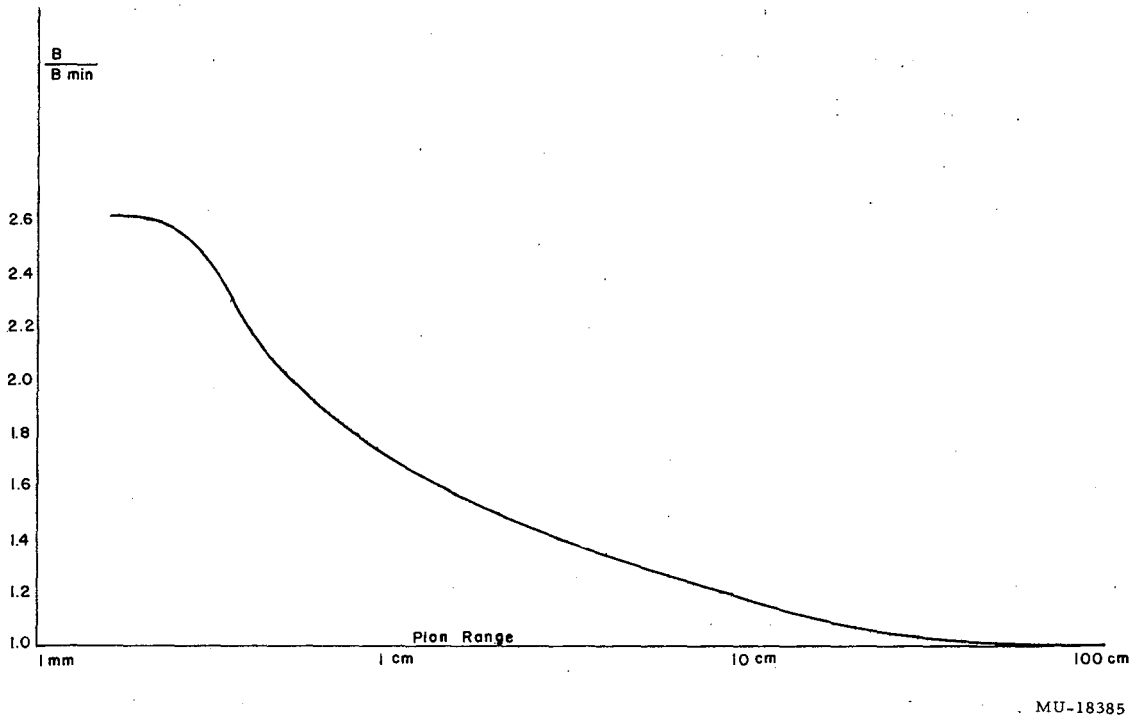

Fig. 4. Blob density vs pion residual range.

$H_\delta = Be^{-gD(\sec \delta - 1)}$ blobs per unit length of track, or

$H_\delta = \frac{1}{\cos \delta} Be^{-gD (\sec \delta - 1)}$ blobs per unit unit length projected.

Thus the true blob count is

$$B = H_\delta \cos \delta \, e^{gD(\sec \delta - 1)},$$

where D is the average grain diameter. The correction factor $\cos \delta \, e^{gD(\sec \delta - 1)}$ is plotted as a function of the dip angle in for various values of gD Fig. 6. It has been checked by blob counts on stopping pions at dip angles up to 60 deg. The value $gD = 0.15$ for minimum ionization best fits the data. The K^- mesons that decayed within 5 mm of the mean stopping line were ionization-counted, and the lacunarity was chosen as the best measure of ionization in this range. Calibration curves were run on stopping K mesons for this determination and to establish the maximum blob density. The variation of lacunarity with K^- - meson residual range is shown in Fig. 7.

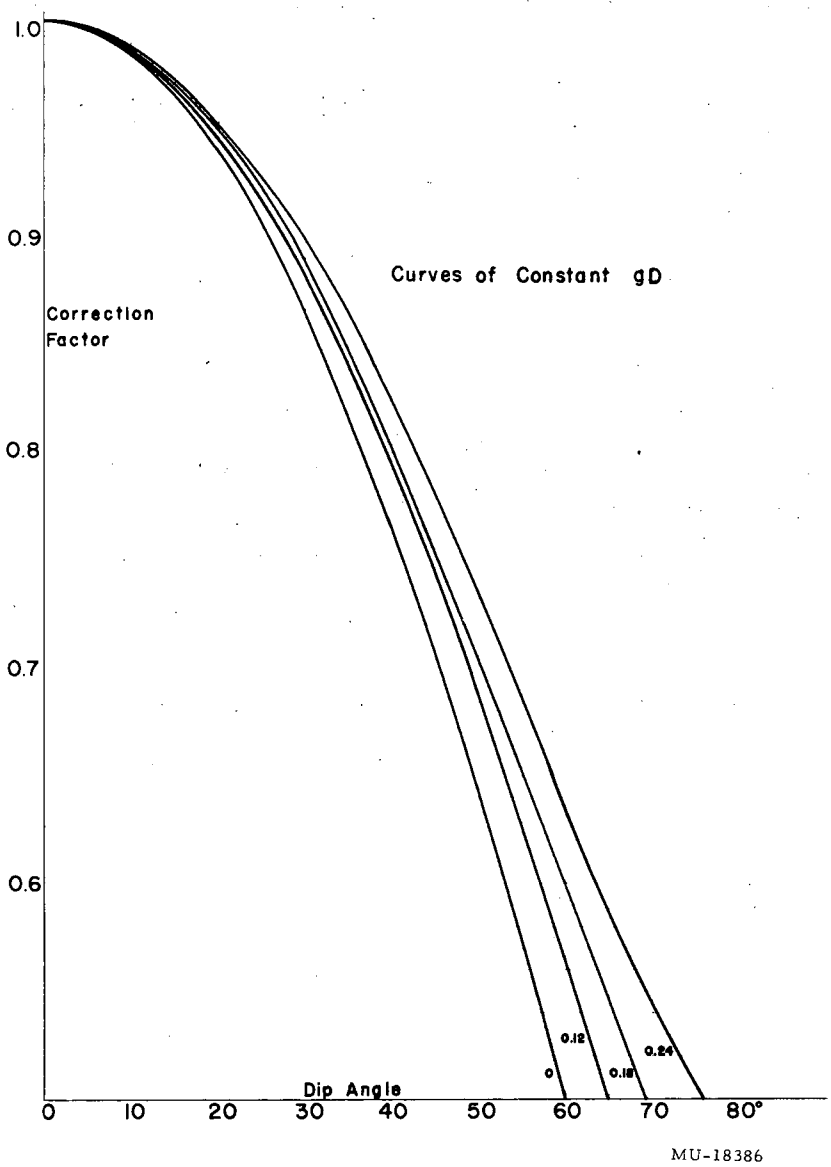

Fig. 6. Correction factor for blob density vs dip angle.

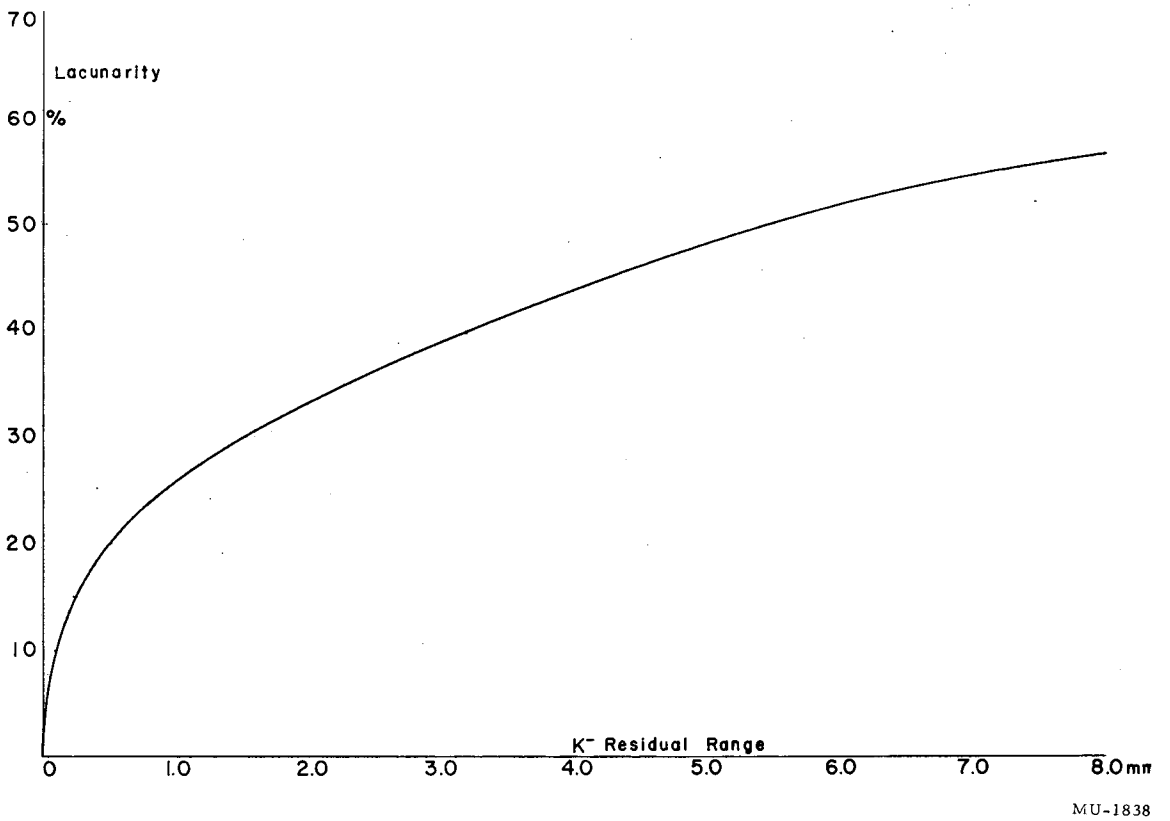

Fig. 7. Lacunarity vs K^- residual range.

RESULTS AND DISCUSSION

Of the 2582 K^- mesons followed in the 2B stack, 2156 came to rest and interacted and 426 made stars in flight. Of the in-flight events, 48 had one lightly ionizing secondary and no blob or Auger electron and were classed as decaylike events; 38 had no visible secondary or blob or electron and were called disappearances in flight. Each of the decaylike events whose secondary could be a pion is a possible K^--meson interaction in flight, and each of the disappearances in flight is a possible decaylike event with an undiscovered near-minimum-ionizing secondary.

Table I shows the results of the measurements on the 48 decaylike events. The second column of this table lists the K^--meson residual ranges to the mean stopping line at the decay point, or the ranges determined from ionization measurements for those less than 5 mm. The third column lists the K^--meson momenta determined from the residual ranges. In column 4 are given the projected angles between the directions of the K mesons and their secondaries, and columns 5 and 6 list the dip angles of these tracks. The space angles computed from these measurements are given in column 7. Column 8 gives the terminal behavior of the secondary track--i.e., whether they come to rest, interact in flight, or leave the stack. Notations on distinguishing behavior, such as large-angle scatterings, are also listed in this column. Column 9 gives the lengths of secondary track from decay point to termination. Column 10 lists the results of the blob-density measurements on the secondary in units of minimum blob density, and column 11 gives the distances from the decay point to the point where the blob-density measurement was taken.

The kinematic analyses of these events are presented in Table II, wherein the measured momenta of the secondaries are compared with those computed from the K^--meson momentum, the angle measurements, and assumed modes of decay. Only the decay modes established for K^+ mesons were considered. Columns 2 through 6 list the secondary momenta for relevant decay modes computed from the information in

Table I

Results of Measurements on the Decaylike events

Event	K-Meson Data		Angle Measurements (degrees)				Secondary Data			
	R_k (cm)	P_k (Mev/c)	ϕ_{ks}	δ_k	δ_s	θ	Terminal behavior	Track length (cm)	Blob density	ΔR(cm)
1	1.46±0.19	225.5±8.5	105.5	1.9	-10.4	105.6±0.5	0-prong star at rest	2.03±.06		
2	0.06±0.02	88.7±7.8	129.6	4.7	-34.3	126.9±1.1	2-prong star at rest	5.93±0.16		
3	0.09±0.03	100.5±8.1	178.8	2.7	11.8	164.8±3.7	1-prong star at rest	3.23±0.09		
4	0.10±0.06	103.0±15.0	109.7	13.5	-68.9	109.3±1.5	1-prong star at rest	7.17±0.19		
5	0.09±0.03	99±10	17.1	6.8	-35.1	44.1±2.9	0-prong star at rest	16.0±0.4		
6	1.83±0.24	241.2±9.4	55.5	22.0	-19.1	65.2±1.8	1-prong star at rest	11.5±0.3		
7	2.75±0.19	273.5±6.1	64.4	20.5	10.5	62.5±7.5	0-prong star at rest	0.153±.010		
8	1.49±.20	227.2±8.4	165.2	5.5	-26.9	154.3±1.0	0-prong star in flight	1.48	1.00±.04	1.06
9	1.60±0.23	231.9±9.1	5.3	0.0	50.0	50.2±4.3	1-prong star in flight	1.24	1.01±.05	0.33
10	0.275±0.270	138^{+31}_{-96}	36.5	13.7	-78.7	94.7±4.0	coplanar π-p scattering	1.16		
11	1.38±0.20	221.8±9.0	20.9	6.9	0.0	22.0±1.0	1-prong star in flight	2.88	1.18±.04	0.2
12	0.51±0.09	163±10	48.1	11.1	16.0	46.9±0.5	0-prong star in flight	6.66	1.11±.04	0.77
13	2.70±0.20	271.9±6.4	24.8	6.8	-11.1	30.5±1.4	4-prong star in flight	5.08	1.05±.04	4.6
14	2.10±0.18	251.6±6.8	108.9	0.9	22.7	107.0±0.6	out stack--16° scattering	9.1	1.75±.07	7.52
15	2.20±0.20	255.5±6.6	9.0	-2.1	-18.0	18.2±1.9	out stack--15° scattering	17.5	1.03±.04	17.2
16	$0.37^{+0.6}_{-0.2}$	150±50	42.3	51.9	-3.8	66.3±1.0	out stack--120° scattering	3.74	1.06±.04	0.2
17	3.37±0.22	291.2±5.9	1.5	24.8	8.3	16.5±3.7	0-prong star in flight	21.26	1.25±.05	20.9
18	2.34±0.20	260.3±6.4	151.5	2.6	7.9	149.7±2.2	out stack--10° scattering	1.49	1.75±.07	0.2
19	0.29±0.20	140^{+23}_{-41}	21.5	3.5	61.7	60.4±2.2	energy loss and scattering	0.64	1.15±0.4	0.2
20	0.58±0.19	171.7±14.9	13.1	0.0	22.1	25.6±2.9	out stack	22.5	1.06±.04	19.15
21	1.42±0.21	223.9±.95	20.6	17.1	-20.7	42.8±2.7	out stack	21.9	1.14±0.04	19.8
22	2.31±0.21	259.4±6.7	44.4	4.4	-11.5	46.9±0.6	out stack	21.49	1.075±0.045	19.8
23	0.27±0.20	137^{+24}_{-44}	74.9	-8.9	- 2.5	74.3±0.5	out stack	20.6	1.09±0.04	19.8
24	0.22±0.06	129±10	0.7	-10.8	23.9	34.7±2.3	out stack	20.49	1.14±0.04	19.65
25	1.08±0.19	206.3±10.0	13.9	0.0	25.0	28.4±3.3	out stack	20.16	1.09±.04	19.5
26	1.07±0.23	205.5±12.1	41.5	16.8	14.3	40.0±0.6	out stack	18.95	1.19±.05	18.65
27	0.97±0.19	200.0±10.8	41.8	1.3	17.0	44.0±1.2	out stack	14.11	1.01±.05 1.075±.05	12.6 0.1
28	1.62±0.25	233.0±9.8	17.4	5.4	-21.5	31.9±3.3	out stack	11.8	1.48±0.06	11.52
29	1.00±0.23	201.7±12.6	6.5	10.9	-75.0	62.0±4.0	out stack	11.59	1.35±0.07	11.3
30	1.99±0.21	247.2±7.9	33.4	2.9	-38.7	51.7±2.0	out stack	10.31	0.98±0.05	9.9
31	1.30±0.20	218.1±9.3	130.0	7.5	38.4	114.8±2.4	out stack	9.2	1.11±.04 1.14±.04	4.7 7.9
32	0.24±0.08	132.8±11.6	5.9	25.8	65.5	39.9±3.4	out stack	8.22	1.045±.04	6.77
33	2.09±0.22	251.2±8.3	69.0	-6.6	25.7	74.3±0.7	out stack	8.1	1.50±0.05	7.8
34	0.58±0.23	171.7±17.7	88.5	15.8	-46.5	100.4±1.4	out stack	7.40	1.08±.04	3.37
35	0.62±0.20	174±19	55.8	-16.0	-52.9	56.9±0.8	out stack	6.5	0.97±0.05	6.1
36	2.58±0.25	268.0±8.0	75.6	1.6	-17.7	76.8±0.6	out stack	5.08	1.15±.04	4.8
37	2.65±0.21	270.3±6.7	124.3	4.6	-84.9	97.5±1.4	out stack	4.65	1.15±.04	4.2
38	0.52±0.08	167±9	149.5	10.9	10.9	143.7±1.7	out stack	4.39	1.20±.045	3.7
39	1.06±0.20	205.2±10.9	161.5	12.7	-46.5	151.5±3.5	out stack	3.8	1.11±0.04	3.2
40	1.10±0.23	207.5±11.9	165.7	9.0	17.6	149.8±2.9	out stack	3.34	1.07±.04	0.9
41	0.85±0.25	191.9±15.3	174.2	4.0	7.8	166.8±1.2	out stack	3.25	1.74±.07	2.8
42	2.59±0.24	268.3±7.7	135.8	0.0	-49.8	152.4±3.1	out stack	2.5	1.14±.04	9.96
43	0.59±0.24	172.2±18.2	115.3	31.2	20.6	99.2±3.2	out stack	2.25	1.11±.04	1.9
44	1.72±0.20	237.0±7.7	166.4	-1.8	-35.2	140.8±1.2	out stack	1.90	1.24±.05	0.90
45	1.38±0.20	221.8±9.2	175.0	0.0	40.3	139.5±2.8	out stack	1.90	1.21±.04	0.85
46	2.56±0.20	267.2±6.3	167.0	-16.6	25.7	135.9±3.3	out stack	0.90	1.60±0.06	0.2
47	2.23±0.18	256.4±5.8	170.7	16.1	2.4	159.4±1.2	out stack	0.76	1.00±.04	0.35
48	2.85±0.19	276.5±5.7	149.0	0.0	51.9	121.9±3.8	out stack	0.54	1.09±.05	0.27

Table II

Comparison of computed and measured secondary momenta

	Calculated secondary momentum, assuming decay mode under which listed (Mev/c)					Measured momenta for possible secondary identifications (Mev/c)		
Event	$K_{\mu 2}$	$K_{\mu 3}$	$K_{\pi 2}$	$K_{\pi 3}$	K_{e3}			Modes consistent with
1			154.9±1.2	< 89.0		π^-	105.2±1.0	Interaction
2			178.2±2.2			π^-	154.3±1.6	Interaction
3			160.1±3.9	< 97.4		π^-	123.4±1.2	Interaction
4			183.4±2.5			π^-	166.4±1.7	Interaction
5			238.9±3.7			π^-	235.5±2.8	$K_{\pi 2}$, Interaction
6			217.6±2.4			π^-	202.0±2.3	Interaction
7				< 144.8		π^-	48±1	$K_{\pi 3}$, Interaction
8			116.3±3.7			π	>260	Interaction
9			260.6±10.8			π	345^{+215}_{-50}	$K_{\pi 2}$, Interaction
10			189.1±1.5			π	264±11	Interaction
11			318.0±4.3	< 217.8		π	188±21	$K_{\pi 3}$, Interaction
12			254.4±3.3			π	263^{+44}_{-27}	$K_{\pi 2}$, Interaction
13			322.7±4.6			π	306^{+134}_{-36}	$K_{\pi 2}$, Interaction
14			145.8±1.1			π	238^{+40}_{-25}	Interaction
15			342.7±4.4			π	425^{+235}_{-60}	$K_{\pi 2}$, Interaction
16			223.7±9.5			π	263±40	$K_{\pi 2}$, Interaction
17			366.8±7.5			π	328±22	$K_{\pi 2}$, Interaction
18			107.7±2.6			π	110±7	$K_{\pi 2}$, Interaction
19					< 254	e	>5	K_{e3}
20	322.7±7.7	< 295.9	287.6±7.4			π	390^{+90}_{-35}	$K_{\mu 2}$
						μ	322^{+65}_{-24}	
21	312.5±7.2	< 286.2				π	340±22	$K_{\mu 2}$, $K_{\mu 3}$
						μ	287±21	Interaction
22	309.3±2.8	< 283.1	272.7±2.7			π	374^{+70}_{-28}	$K_{\mu 2}$, Interaction
						μ	313^{+52}_{-25}	
23	244.8±3.2	< 223.6				π	350^{+35}_{-25}	$K_{\mu 2}$, Interaction
						μ	289^{+30}_{-17}	
24	292.1±4.8	< 267.5	258.7±4.6			π	338±17	$K_{\mu 2}$, Interaction
						μ	283±15	

Table II (continued)

Comparison of computed and measured secondary momenta								
	Calculated secondary momentum, assuming decay mode under which listed (Mev/c)					Measured momenta for possible secondary identifications (Mev/c)		
Event	$K_{\mu 2}$	$K_{\mu 3}$	$K_{\pi 2}$	$K_{\pi 3}$	K_{e3}			Modes consistent with
25	336.1±7.0	< 308.2	299.9±6.8			π	362^{+43}_{-24}	$K_{\mu 2}$, $K_{\mu 3}$, Interaction
						μ	300^{+28}_{-25}	
26	313.4±4.7	< 287.1	249.0±4.1			π	418^{+237}_{-68}	$K_{\mu 2}$, $K_{\mu 3}$, Interaction
						μ	355^{+150}_{-70}	
27	303.4±4.6	< 277.9	268.4±4.4			π	411±57	$K_{\mu 2}$, $K_{\mu 3}$
						μ	319±33	
28	341.2±8.3	< 312.8	304.2±8.0			π	220±4	$K_{\mu 3}$, Interaction
						μ	185±3	
29	221.1±4.4	< 201.4	188.9±4.2			π	230^{+15}_{-7}	$K_{\mu 2}$, $K_{\mu 3}$, Interaction
						μ	192^{+11}_{-5}	
30	294.1±6.0	< 269.0	258.3±5.8			π	460^{+210}_{-60}	$K_{\mu 2}$, Interaction
						μ	358^{+104}_{-43}	
31	177.2±3.2	< 160.6	146.5±3.1			π	263±23	$K_{\mu 2}$, Interaction
						μ	205±17	
32	288.8±5.9	<263.8	254.8±5.6			π	326^{+200}_{-42}	$K_{\mu 2}$, $K_{\mu 3}$, $K_{\pi 2}$, Interaction
						μ	256^{+154}_{-33}	
33	236.8±1.8	< 215.8	202.8±1.8			π	192±5	$K_{\mu 3}$, $K_{\pi 2}$, Interaction
						μ	158±4	
34	206.3±2.3	< 187.7	175.3±2.2			π	271^{+42}_{-21}	$K_{\mu 2}$, Interaction
						μ	208^{+27}_{-13}	
35	273.5±5.2	< 250.2	240.1±5.0			π	600±195	$K_{\mu 2}$, $K_{\mu 3}$, $K_{\pi 2}$, Interaction
						μ	458±143	
36	228.7±1.5	< 208.2	194.4±1.5			π	240^{+22}_{-18}	$K_{\mu 3}$, $K_{\mu 2}$, $K_{\pi 2}$, Interaction
						μ	188^{+16}_{-13}	
37	187.1±2.3	< 169.5	154±2.2		< 192	π	235^{+28}_{-20}	$K_{\mu 2}$, $K_{\mu 3}$, K_{e3}, Interaction
						μ	184^{+19}_{-16}	
						e	> 10	

Table II (continued)

Comparison of computed and measured secondary momenta								
	Calculated secondary momentum, assuming decay mode under which listed (Mev/C)					Measured momenta for possible secondary identifications (Mev/c)		
Event	$K_{\mu 2}$	$K_{\mu 3}$	$K_{\pi 2}$	$K_{\pi 3}$	K_{e3}			Modes consistent with
38	171.1±3.7	< 155.1	141.9±3.6			π	210±22	$K_{\mu 2}$, $K_{\mu 3}$, Interaction
						μ	157±20	
39	177.0±4.3	< 160.5	146.6±4.1			π	253±28	$K_{\mu 2}$, Interaction
						μ	195±20	
40	153.9±5.3	< 139.0	107.2±5.0			π	264±33	$K_{\mu 2}$, Interaction
						μ	200±26	
41	158.8±7.7	< 139.0	125.0±7.4			π	127±5	$K_{\pi 2}$, $K_{\mu 3}$, Interaction
						μ	104±3	
42	159.9±3.9	< 144.3	128.5±3.7		< 164	π	224^{+21}_{-24}	$K_{\mu 2}$, K_{e3}, Interaction
						μ	170^{+15}_{-15}	
						e	> 10	
43	207.7±4.3	< 189.0	176.6±4.1		< 211	π	244±28	$K_{\mu 2}$, $K_{\mu 3}$, $K_{\pi 2}$, K_{e3}, Interaction
						μ	187±20	
						e	> 10	
44	149.2±3.0	< 134.6	119.5±2.8			π	170±21	$K_{\mu 2}$, $K_{\mu 3}$, $K_{\pi 2}$, Interaction
						μ	187±20	
45	154.8±3.8	< 139.8	125.2±3.7			π	187±22	$K_{\mu 2}$, $K_{\mu 3}$, $K_{\pi 2}$, Interaction
						μ	143±15	
46	143.5±3.2	< 129.1	113.2±3.0			π	102±8	$K_{\pi 2}$, $K_{\mu 3}$, Interaction
47	134.7±2.8	< 121.0	105.4±2.7			π	> 238	Interaction
						μ	> 168	
48	152.9±4.3	< 137.8	121.7±4.0		< 158	π	237^{+53}_{-28}	$K_{\mu 2}$, K_{e3}, Interaction
						μ	178^{+44}_{-22}	
						e	> 5	

columns 3 through 6 of Table I. Column 7 lists the measured momenta of the secondaries derived from the information in columns 10 and 11 of Table I for all possible identities of the secondary. For the first nineteen events listed the secondary is identified by the information given in column 8 of Table I. Four of the secondaries left the stack a short distance from the decay point, with ionization near the plateau, and therefore could be electrons. All of these were too steep for multiple-scattering measurements. Column 8 of Table II lists the modes with which the event is consistent, with the most probable mode listed first. As can be seen, most of the events are consistent with more than one mode, and in addition each event whose secondary could be a pion is a possible nuclear interaction.

To determine the distribution of the decaylike events among the modes considered -- $K_{\mu 2}$, $K_{\mu 3}$, $K_{\pi 2}$, $K_{\pi 3}$, K_{e3}, and nuclear interaction -- a probability matrix, P, of which an element P_{ij} gives the relative probability that the ith event belongs to the jth mode, was derived and normalized to $\Sigma_j P_{ij} = 1$. Then $\Sigma_i P_{ij}$ is the population of the jth mode. The P_{ij} were determined graphically as shown in Fig. 8 by plotting for each event the computed secondary momenta for the relevant modes from columns 2 through 6 of Table II. The two-body momenta were plotted as normal probability curves and the three-body spectra were approximated by means of triangles with maximum probability at two-thirds of the maximum momentum. On the same graph the probability distributions of momentum from the measurements on the secondary (columns 8 and 9 of Table II) were drawn. All curves were normalized to unit area. Product curves of the ordinates of the computed and measured momenta curves were drawn, and the areas under these determine the relative probabilities of the modes. The spectrum used for the π^- from nuclear interactions in flight is that shown in Fig. 9. Eisenberg et al.[22] have calculated the spectrum of π^- expected from the in-flight interactions

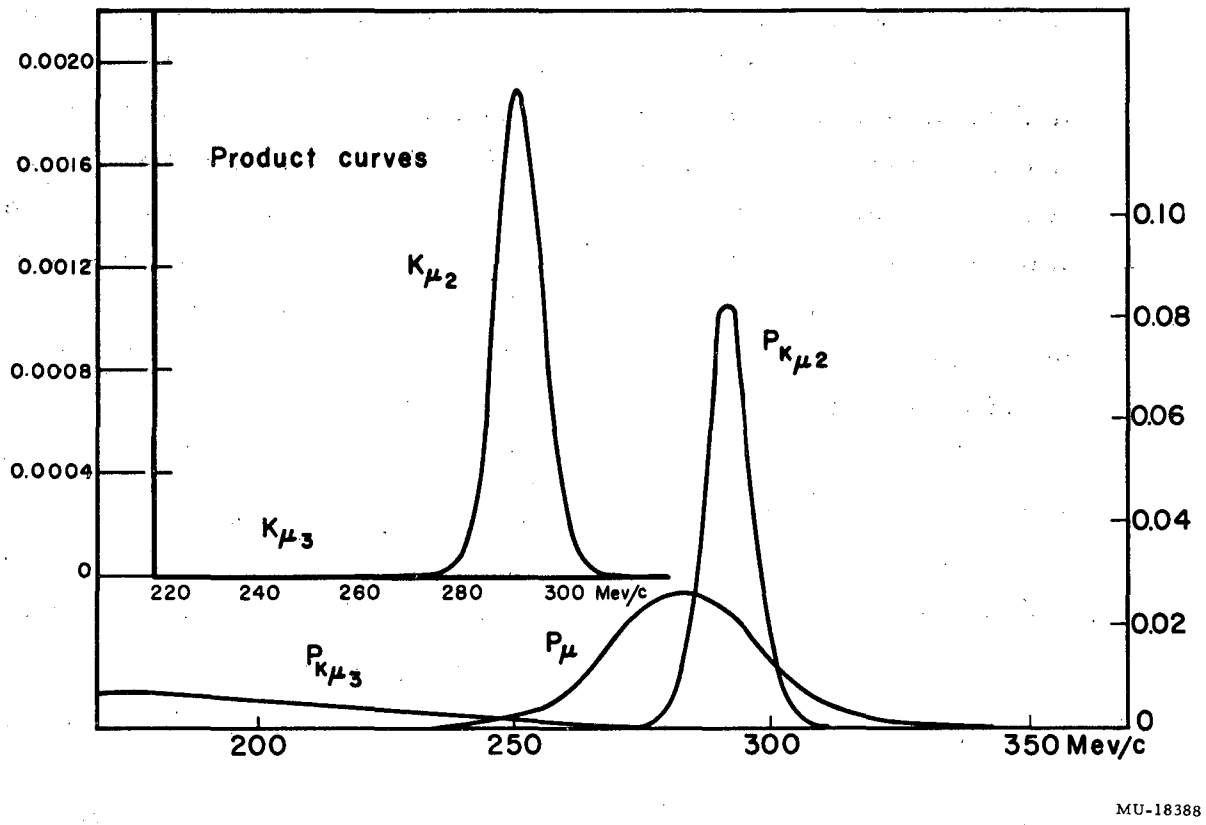

Fig. 8. Momentum probability distribution.

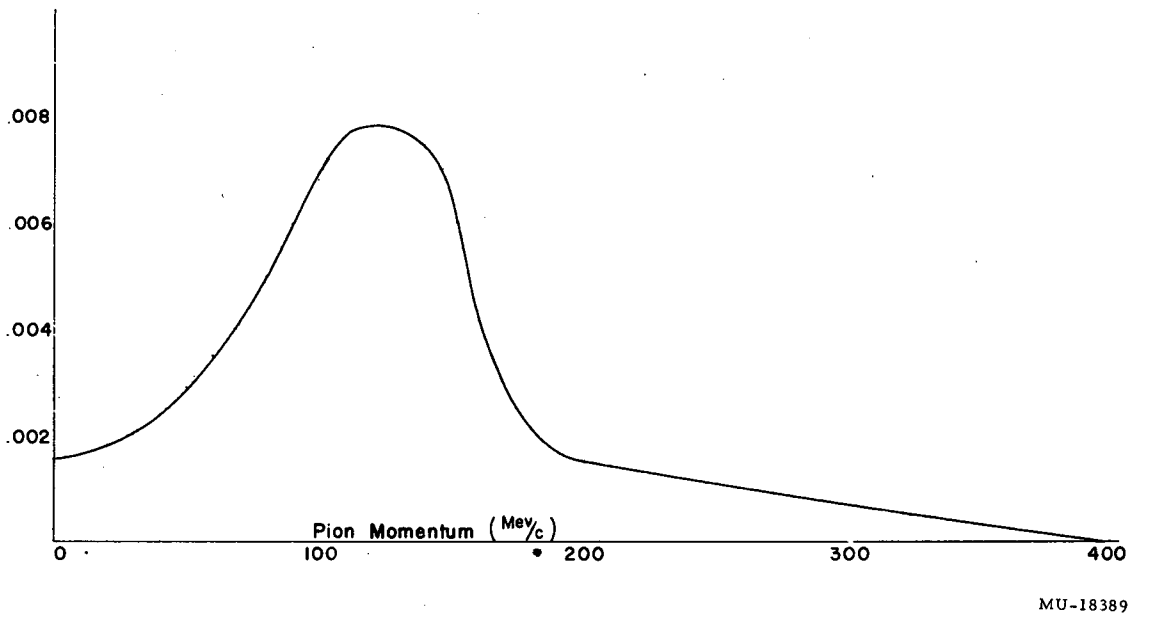

Fig. 9. Spectrum of π^- from K^- interactions in flight.

$$K^- + n \rightarrow \pi^- + \Lambda^0$$

$$\rightarrow \pi^- + \Sigma^0$$

for pion energies up to 100 Mev and for K^- meson energies from 5 to 150 Mev, taking into account scattering of the pion in the nucleus. These curves are roughly the same and agree with the spectrum of pions observed by them. The curve used here is their curve for $\Lambda\pi$ production plotted against momentum and made to decrease linearly to zero at 395 Mev/c, the maximum pion momentum obtainable at the K^--meson energies under consideration. The shape of this curve beyond 100 Mev (195 Mev/c) and the maximum momentum are not critical since the lower energies are more probable and the probabilities involved are small in relation to those of the decay modes with which they are being compared. This is borne out by the decaylike interactions observed in this study. One further piece of information is available for those events whose secondaries left the stack without having suffered nuclear scatterings and could therefore be pions or muons. The probability of a pion's traveling a distance x in emulsion without interacting with a nucleus is $e^{-x/\lambda}$, where λ is the mean free path. Therefore, the relative probabilities for the pion mode should be multiplied by the factor $\epsilon^{-x/\lambda} / (1 + \epsilon^{-x/\lambda})$, and those for the muon by $1/(1 + \epsilon^{-x/\lambda})$. Since the mean free path in emulsion for a muon scattering greater than 7 deg is 18 meters,[23] this possibility can be neglected. A similar argument holds for events consistant with the K_{e3} mode. An electron is recognized by its characteristic energy loss and scattering. The radiation length in emulsion, 2.91 cm, has been taken here as a mean free path for an identifying energy loss by an electron. The areas under the product curves multiplied by the appropriate distance factors are then normalized to unit total probability to give the P_{ij} presented in Table III. The distribution of the decaylike events is then given by the totals (p. 38) from Table III.

Table III

Probability distribution of decaylike events

Event	$K_{\mu 2}$	$K_{\mu 3}$	$K_{\pi 2}$	$K_{\pi 3}$	K_{e3}	Interaction
1						1.00
2						1.00
3						1.00
4						1.00
5			0.98			0.02
6						1.00
7				0.71		0.29
8						1.00
9			0.83			0.17
10						1.00
11				0.62		0.38
12			0.91			0.09
13			0.93			0.07
14						1.00
15			0.98			0.02
16			0.84			0.16
17			0.89			0.11
18			0.86			0.14
19					1.00	
20	1.00					
21	0.91	0.05				0.04
22	0.99					0.01
23	0.75					0.25
24	0.99					0.01
25	0.98	0.02				
26	0.93	0.06				0.01
27	0.99	0.01				
28		0.88				0.12
29	0.60	0.23				0.17
30	0.99					0.01
31	0.89					0.11
32	0.74	0.10	0.13			0.03
33		0.47	0.45			0.08
34	0.96					0.04
35	0.65	-.10	0.17			0.08
36	0.14	0.52	0.17			0.17
37	0.88	0.01			0.07	0.04
38	0.81	0.12				0.07
39	0.93					0.07
40	0.78					0.22
41		0.19	0.69			0.12
42	0.81				0.14	0.05
43	0.66	0.08	0.06		0.13	0.07
44	0.60	0.17	0.04			0.19
45	0.85	0.05	0.01			0.09
46		0.34	0.49			0.17
47						1.00
48	0.57				0.32	0.11

The spectrum used for pions from interactions was calculated for all interactions in flight, and may not be correct for decaylike interactions, as it might be expected that the pions from them would have scattered less within the nucleus and would leave the nucleus with greater energy. However, Eisenberg et al.[22] find that the pions from events in flight with no stable prongs seem to have the same spectrum as those from all events in flight, which would indicate they do scatter as much. The decaylike interactions in this study are also consistent with this assumption, although not enough data have been obtained in either study to determine the pion spectrum of decaylike interactions. So that the effect of this spectrum on the final results might be seen, the P_{ij} were determined for an extreme case--a uniform spectrum from 100 to 400 Mev/c. This yielded a total of 17.53 interactions among the 48 decaylike events, compared with 12.78 for the spectrum used. Eisenberg et al.[10] have analyzed K^--meson–nuclear interactions in flight which have a blob and one pion secondary, and find that 70% do not fit the kinematics of either of the two-body decay modes. Nine of the decaylike events were not consistent with any mode, which would predict a total of 12.9 decaylike interactions if the ratios are the same for events with and without blobs.

The decaylike events are not an unbiased sample, because the secondaries missed are most probably the more lightly ionizing two-body modes. The problem of the undetected secondaries was complicated by differing minimum blob densities in the different development batches and a particularly low blob density in one of them. Each of the disappearances in flight was re-examined twice by competent observers; three additional secondaries were found on the first rescan and one on the second rescan. The efficiency of the scanners for detecting the electrons from muon decays was determined previously to be better than 95% in pellicles with a minimum blob density near that of the highest in the 2B stack (19 blobs per 100 microns). However, three factors act to lessen the

efficiency for finding the secondaries from decaylike events: First, the scanner knows there is a secondary from the muon decay, whereas the K meson in flight may or may not have a secondary. Second, the decay point of the muon is well defined, while that of the K meson in flight may be several microns from the last blob. Additionally, the electron from muon decay is at plateau ionization, which is approximately 15% above minimum. It is difficult to estimate how much these effects and the lower minimum blob density decrease the efficiency for detecting secondaries.

One estimate of a lower limit to the number of missed decay secondaries may be made from the angular distribution of those detected. Figure 10 shows the distribution of the cosine of the angle between the K meson and the secondary in the center-of-mass system for all of the two-body decays. These, of course, would be expected to be isotropic, and decay secondaries missed would most probably be those of $K_{\mu 2}$ or $K_{\pi 2}$ since they contribute the majority of decays and their secondaries are lighter in ionization. A χ^2 test gives a probability less than 0.02 that a uniform distribution would give deviations larger than shown in Fig. 10. Eight decays added in the region $-0.5 < \cos\theta < 0$ would make this distribution uniform. The secondaries in the region $-0.5 < \cos\theta < 0.5$ are those most likely to be missed because those with $\cos\theta$ less than -0.5 will be emitted more slowly in the lab system and hence have a higher grain density, while those with $\cos\theta > 0.5$ will tend to be flat.

Figure 11 shows the dip-angle distribution of those secondaries emitted with a c.m. angle between -60 deg and +60 deg. Again, within statistics, we would expect an even distribution from -90 to +90 deg. Although there are fewer events in this group, a definite bias for detecting secondaries with dip angles between +30 and -30 deg is evident. Here too, approximately eight additional events with dip angles steeper than 30 deg would be required for axial symmetry. As mentioned before, these estimates would be lower limits to the number of missing decay secondaries, as they are made with the

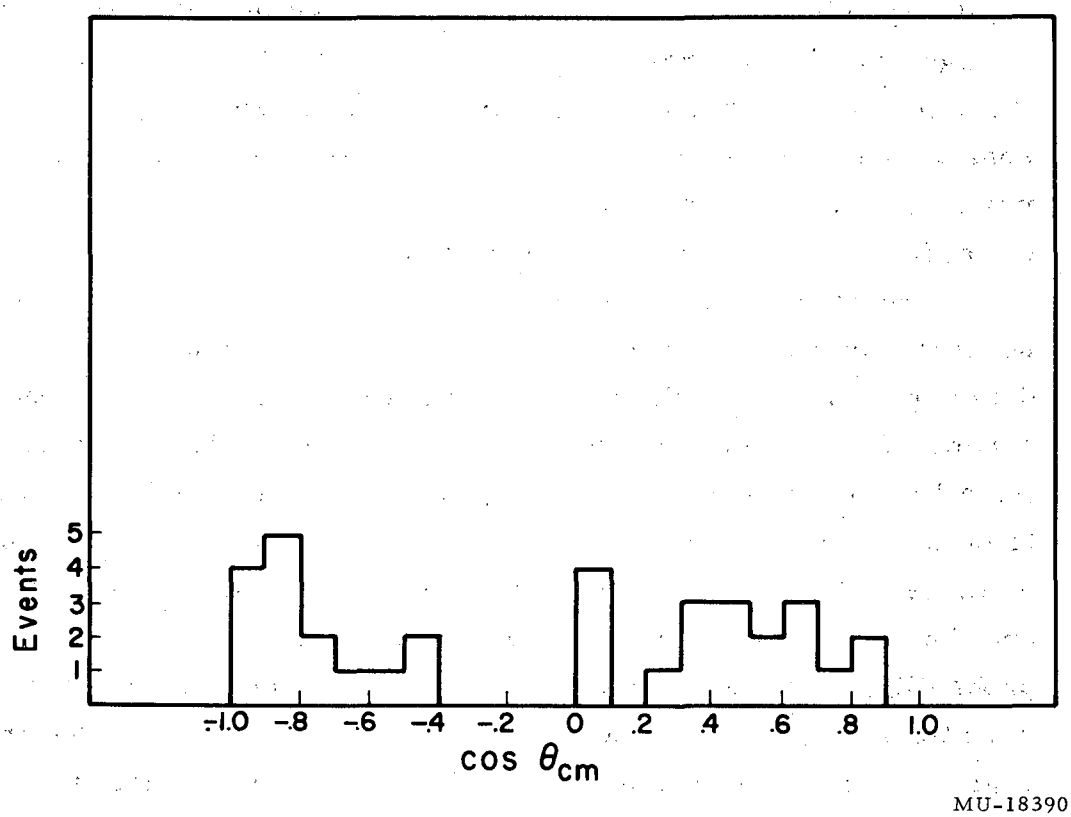

Fig. 10. Cosine of c.m. angle for two-body decays.

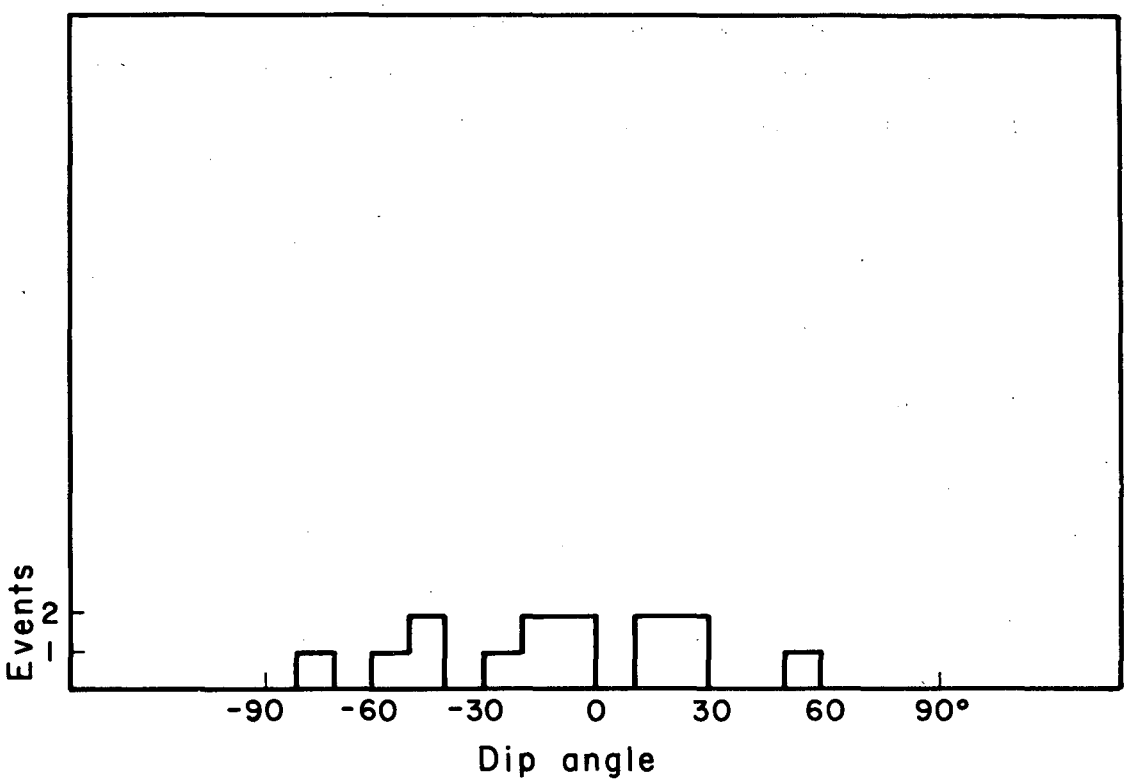

Fig. 11. Dip angle of equatorial two-body decays.

assumption of 100% efficiency for detecting secondaries emitted with a c.m. angle greater than 120 deg or less than 60 deg.

An estimate of an upper limit to this number may be made as follows. Thirteen decaylike nuclear interactions were found which presumably represent the reactions

$$K^- + n \rightarrow \Lambda^0 + \pi^-$$

$$\Sigma^0 + \pi^-.$$

Since there are 1.24 times as many neutrons as bound protons in emulsion, we would expect 11 true disappearances in flight from the reactions

$$K^- + p_{bound} \rightarrow \Lambda^0 + \pi^0$$

$$\rightarrow \Sigma^0 + \pi^0.$$

From the 81 meters of K^--meson track followed we would expect two interactions on free hydrogen of the type

$$K^- + p \rightarrow Y^0 + \pi^0$$

and one charge-exchange scatter. This same ratio among the "clean" interactions with bound protons would predict five true disappearances from charge-exchange scatterings on bound protons. This predicts a total of 19 true disappearances or 19 undetected secondaries. Of the decaylike events with secondaries of ionization less than that of a 10-cm pion, 20% are nuclear interactions. This same ratio among the undetected secondaries would leave a total of 15 undetected decay secondaries.

A third estimate (which is probably not as reliable) can be made by comparing the percentage of clearn zero-prong interactions at rest with that of the in-flight interactions. This ratio is $\frac{146}{2156} = 0.068$, which would predict 25 disappearances in flight and 13 undetected

secondaries if these ratios could be expected to be the same. The first two estimates seem much more reliable, however, and their average, 11.5±3.4, will be used as the best estimate of the number of undetected decay secondaries. These are divided among the decay modes in the same ratio as the analyzed decaylike events with ionization less than that of a 10-cm pion: 60.7% $K_{\mu 2}$, 8.9% $K_{\mu 3}$, 24.8% $K_{\pi 2}$, and 5.6% K_{e3}. This gives the following for the total population of each mode.

	Decaylike events	Undetected secondaries	Total
$K_{\mu 2}$	19.40	6.98	26.4±5.1
$K_{\mu 3}$	3.40	1.02	4.4±2.1
$K_{\pi 2}$	9.43	2.85	12.3±3.5
$K_{\pi 3}$	1.33	0.00	1.3±1.2
K_{e3}	1.66	0.64	2.3±1.5
All	35.22	11.50	46.7±6.8

No τ^- mesons were found in this study, although they have of course been seen by others[10, 11] and are the most easily detected decay mode. The likelihood of there being n events when none are observed is given by e^{-n}, which gives a maximum likelihood of zero with an rms spread of 1.0. We have, finally, the percent relative abundances:

$K^-_{\mu 2}$	$K^-_{\mu 3}$	$K^-_{\pi 2}$	$K^-_{\pi 3}$	K^-_{e3}	τ^-
56.5±7.3	9.5±4.3	26.3±6.6	2.8±2.4	4.9±3.2	0.0±2.1

Only the statistical errors have been included.

The Lifetime Calculation

The proper time during which a K^- meson could have decayed and been detected was derived as follows. In each 5 mm across the face of the stack the distance along the beam direction from the pickup to the mean stopping point was used to determine the mean proper time in each segment, from the tables of Barkas and Young.[24] This multiplied by the number of stopping K mesons was the total proper time for mesons that came to rest. For the in-flight events the residual proper time was subtracted from the mean proper time. From the 2156 K^- mesons that came to rest the total proper time was 5.911×10^{-7} sec, and from the 426 in-flight events the total was 4.96×10^{-8} sec, making a grand total of 6.407×10^{-7} sec. For the lifetime calculation we eliminate from consideration the segment of track at the end of its range in which a K^- meson, had it decayed, might have been considered to be at rest. This was estimated to be 0.3 mm, and none of the decaylike events was in this range. We also eliminate from consideration the first mm of track from the pickup line, since events in this region could not be distinguished from neutron-induced stars with outgoing prongs and were not recorded in the initial scanning. These corrections leave a total proper time of 6.057×10^{-7} sec, and 46.7±6.8 decays, which yields for the K^--meson mean lifetime $1.30^{+0.22}_{-0.17} \times 10^{-8}$ sec.

Since secondaries from events near the top and bottom surface are more likely to escape detection, the lifetime calculated with the top and bottom surfaces of each pellicle excluded is probably less subject to systematic error. Only two of the decaylike events lie within 30 microns of either surface, whereas from a uniform distribution we would expect five. Three of the disappearances in flight lie in this region. Excluding the top and bottom 30 microns of unprocessed emulsion leaves a total proper time of 5.485×10^{-7} sec, 33.5 decays from the decaylike events, and 10.5 decays with undetected

secondaries, or a total of 44.0±6.6 decays. This yields $1.25^{+0.22}_{-0.17} \times 10^{-8}$ sec for the K^--meson mean lifetime.

The lifetime value is in excellent agreement with that of the K^+ meson, $1.223 \pm 0.013 \times 10^{-8}$ sec,[9] and the relative abundances are in reasonably good agreement with the values determined by Birge et al.[5] and by Alexander, Johnson, and O'Ceallaigh,[6] except for that of the τ^- mode, which is considerably lower than the τ^+ abundance quoted by either group, and the $K^-_{\mu 3}$ abundance, which is higher than either $K^+_{\mu 3}$ abundance but within one standard deviation of that quoted by Alexander, Johnson, and O'Ceallaigh.

Because of the limited number of events available for analysis in this study, the statistical errors are too large to definitely establish that the K^--meson lifetime and relative abundances are identical with the corresponding K^+-meson quantities. However, the results are consistent with these identities, which are required by PCT invariance if the K^+ and K^- mesons are particle and antiparticle.

ACKNOWLEDGMENTS

I am particularly indebted to Dr. Walter H. Barkas for suggesting and guiding this research. I am grateful to Dr. Robert Thornton for his interest and encouragement.

It is a pleasure to thank the scanners who found the events and aided in the measurements, particularly Miss Ernestine Beleal, Mrs. Hester Yee, and Mr. Alan Betz for their competent assistance in following and blob-counting the decay secondaries.

To Mrs. Penny Vedder I express my gratitude for programming the decay kinematics calulation and aiding in the IBM 650 computations.

My sincere appreciation to Mr. James Hodges for the construction of the ionization microscope and to Mr. Thomas Taussig for the design of the ionization tabulator.

I should like to thank the members of the Barkas group and the Bevatron crew and all those who helped develop the K^--meson beam and aided in the exposure.

Finally, to my wife, Joyce, for her continued enthusiasm and encouragement and significant help in all phases of this work, my deepest appreciation.

This work was done under the auspices of the U. S. Atomic Energy Commission.

APPENDIX I

Kinematic Curves

Kinematic curves for the $K_{\mu 2}$, $K_{\mu 3}$, $K_{\pi 2}$, and $K_{\pi 3}$ modes of decay are presented as Figs. 12-15. These curves are solutions of the equation

$$E_1 E_2 - P_1 P_2 \cos \theta = C,$$

where the subscripts 1 and 2 refer to the primary and charged secondary and

$$C = 1/2 \, (M_1^2 + M_2^2 - M_n^2)$$

is a function of the masses of the one neutral and two charged particles involved. For the three-body modes the maximum momentum of the secondary is shown. These curves were computed with an IBM 650 program supplied by Dr. Howard White.

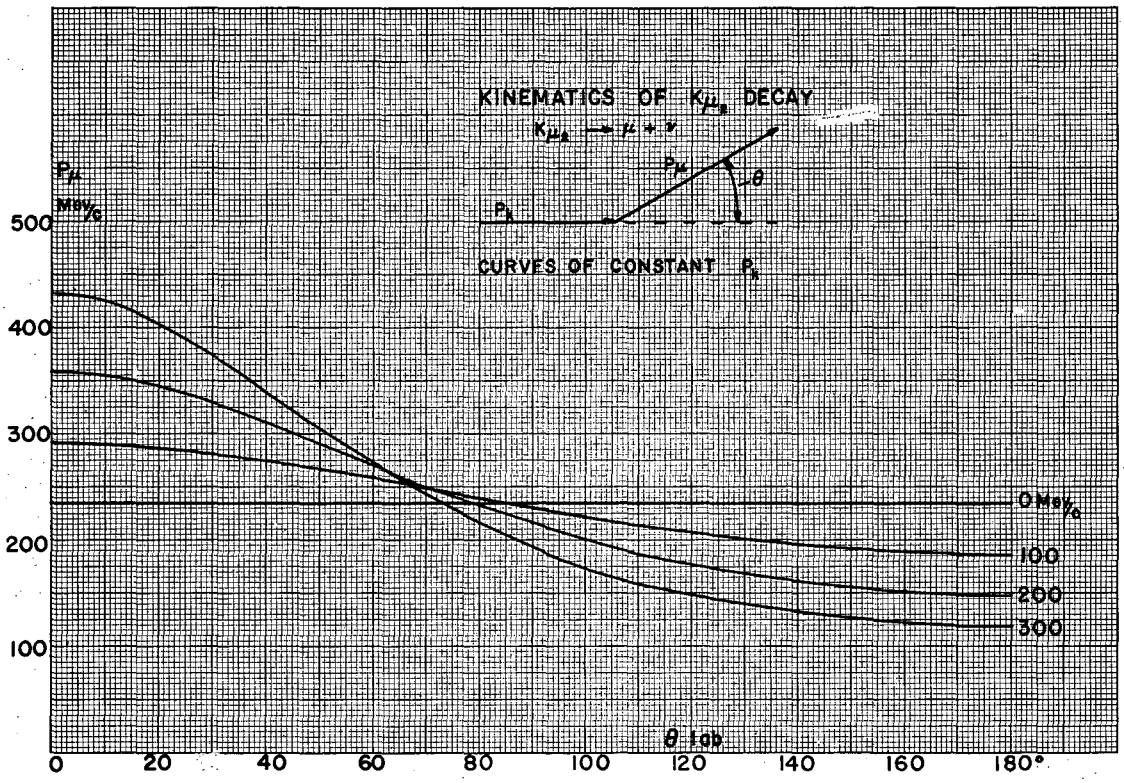
KINEMATICS OF K_{μ_3} DECAY
$K_{\mu_3} \rightarrow \mu + \nu$
P_μ
P_K
θ
CURVES OF CONSTANT P_K
P_μ Mev/c
500
400
300
200
100
0 Mev/c
100
200
300
θ lab
0
20
40
60
80
100
120
140
160
180°

MU-18392

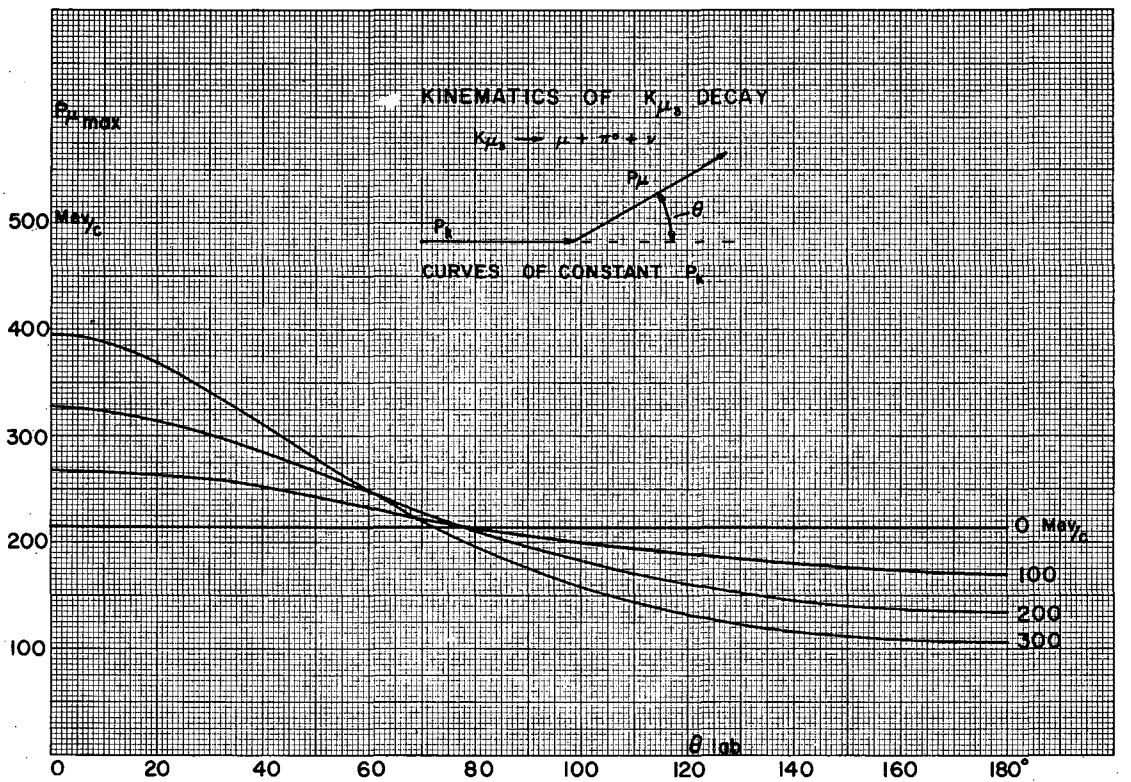
KINEMATICS OF $K_{\mu 3}$ DECAY
$K_{\mu 3} \rightarrow \mu + \pi^0 + \nu$
P_μ
θ
P_k
CURVES OF CONSTANT P_k
$P_{\mu\,max}$
500 Mev/c
400
300
200
100
0 Mev/c
100
200
300
θ lab
0
20
40
60
80
100
120
140
160
180°

MU-18393

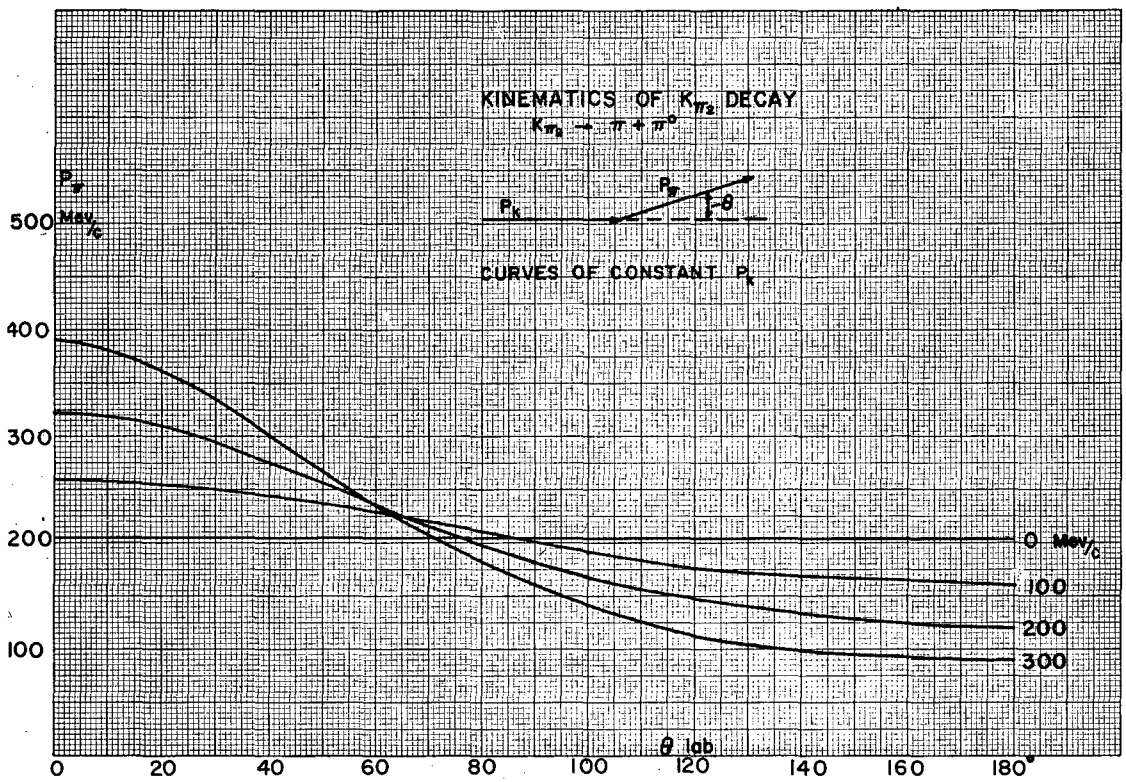
KINEMATICS OF K_{π_2} DECAY
$K_{\pi_2} \rightarrow \pi + \pi^o$
P_π
P_K
θ
CURVES OF CONSTANT P_K
P_π Mev/c
500
400
300
200
100
0 Mev/c
100
200
300
θ lab
0
20
40
60
80
100
120
140
160
180°

MU-18394

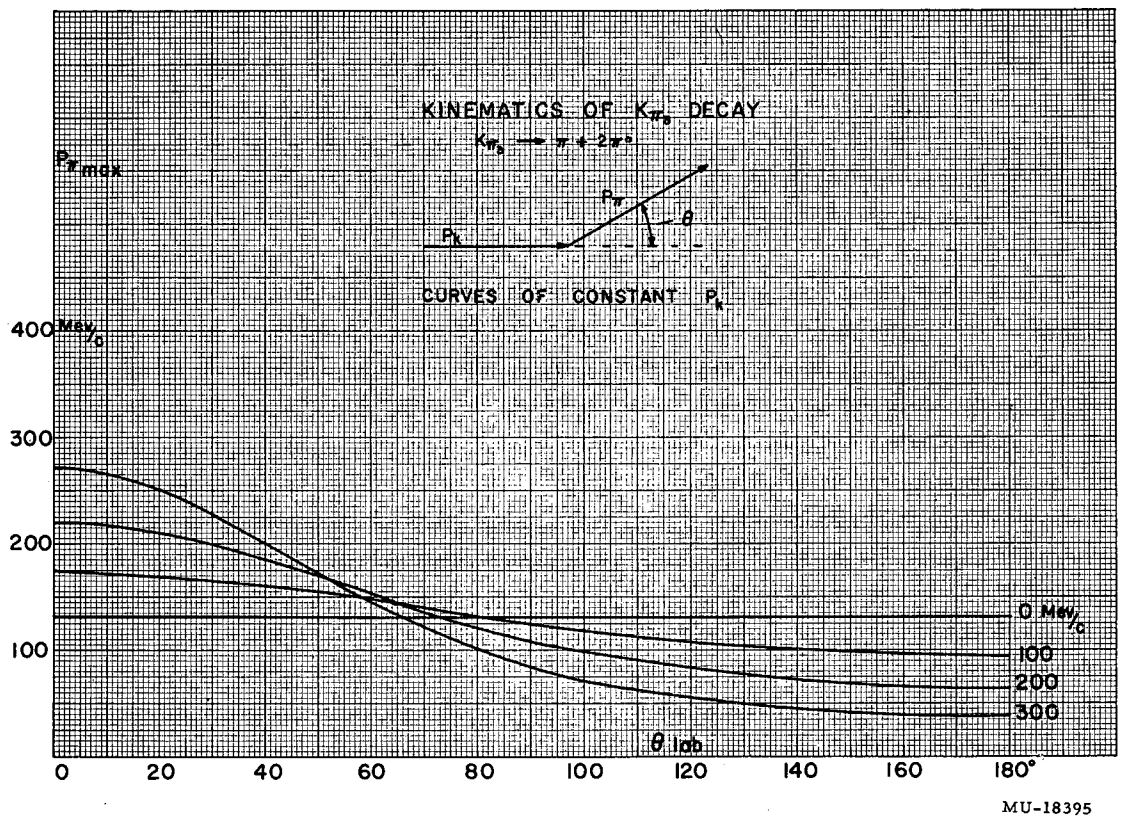
KINEMATICS OF K_{π_3} DECAY
$K_{\pi_3} \rightarrow \pi + 2\pi^0$
$P_{\pi max}$
P_π
θ
P_K
CURVES OF CONSTANT P_K
400 Mev/c
300
200
100
0 Mev/c
100
200
300
θ lab
0
20
40
60
80
100
120
140
160
180°
MU-18395

APPENDIX II

Ionization-Data Microscope and Tabulator

Since ionization determinations constitute a large part of the measurements taken in emulsion work, it is desirable to improve the speed, objectivity, and ease of making them. The apparatus described here was built for this purpose, and has proved to be of great value in this work. It consists of a specially modified microscope and an electronic data tabulator, and borrows heavily from a device described by Baroni and Castagnoli.[25]

A constant-speed reversible electric motor drives the x movement of the microscope stage through gears at 40 and 200μ/min. To aid in alignment of tracks with the x movement, a rotator with vacuum hold-down for the plate is mounted on the condenser frame, permitting a 60-deg rotation of the plate about the optic axis. Vacuum hold-downs on the stage also are provided so that the plate may be fixed to it without risk of disturbing the aligment.

The tabulator is a transistorized modification of the circuit used by Baroni and Castagnoli.[25] On one traversal of the track, it tabulates upon the operation of one push button, the total number of gaps, the number of gaps greater than a preset length, and the integrated gap length. The tabulator is turned on by a foot switch simultaneously with an electric clock, which indicates the total time, or length of track scanned. The push button is depressed as the beginning of a gap crosses a line on the reticle and released at the end of a gap. This switch operates a second clock which integrates gap length, a counter which totals gaps and through a variable RC circuit, the long-gap counter. The instrument is shown in Fig. 16.

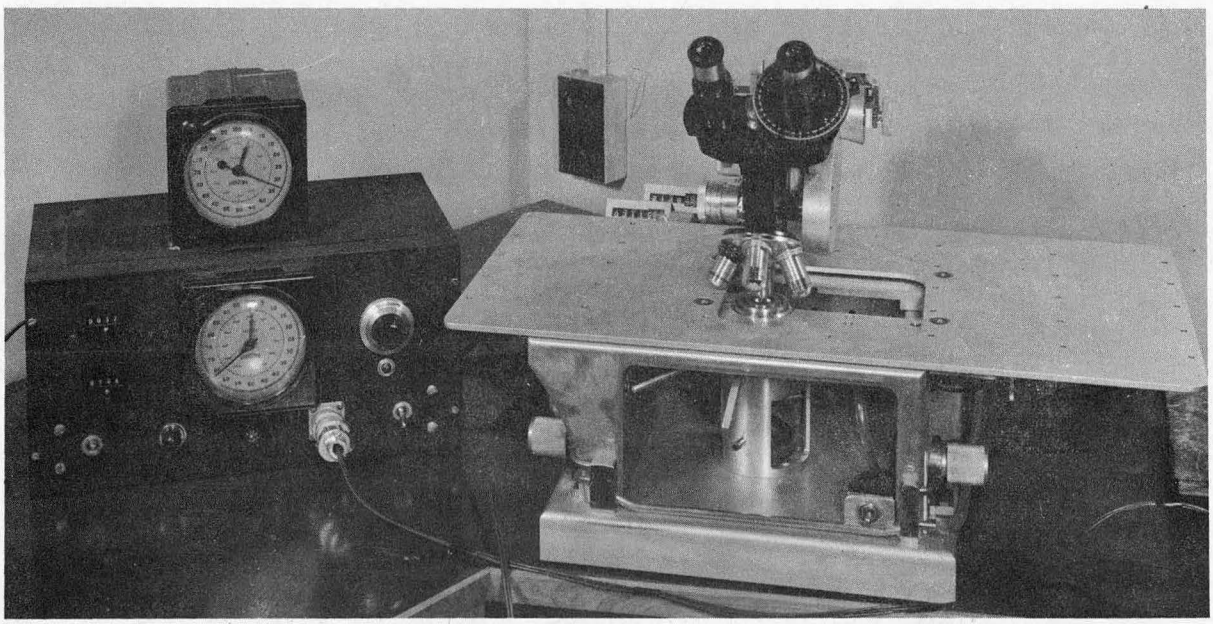

ZN-2244

Fig. 16. Ionization-data microscope and tabulator.

REFERENCES

1. L. W. Alvarez and S. Goldhaber, Nuovo cimento 2, 344 (1955).
2. Iloff, Chupp, Goldhaber, Goldhaber, Lannutti, Pevsner, and Ritson, Phys. Rev. 99, 1617 (1955).
3. Orear, Harris, and Taylor, Phys. Rev. 104, 1463 (1956).
4. Bhowmik, Evans, Nilsson, Prouse, Biswas, Cecarelli, Waloschek, Hooper, Grilli, and Guerriero, Nuovo cimento 5, 994 (1957).
5. Birge, Perkins, Peterson, Stork, and Whitehead, Nuovo cimento 4, 834 (1956).
6. Alexander, Johnson, and O'Ceallaigh, Nuovo cimento 6, 478 (1957).
7. R. Motley and V. Fitch, Phys. Rev. 105, 265 (1957).
8. Alvarez, Crawford, Good, and Stevenson, Phys. Rev. 101, 503 (1956).
9. W. H. Barkas and A. H. Rosenfeld, Data For Elementary-Particle Physics, UCRL-8030, March 1958.
10. Eisenberg, Koch, Lohrmann, Nikolic, Schneeberger, and Winzeler, Nuovo cimento 8, 663 (1958).
11. S. Nilsson and A. Frisk, Ark. Fys, 14, 293 (1958).
12. Iloff, Goldhaber, Goldhaber, Lannutti, Gilbert, Violet, White, Fournet, Pevsner, Ritson, and Widgoff, Phys. Rev. 102, 927 (1956).
13. Barkas, Dudziak, Giles, Heckman, Inman, Mason, Nickols, and Smith, Phys. Rev. 105, 1417 (1957).
14. J. Hornbostel and G. T. Zorn, Phys. Rev. 109, 165 (1958).
15. T. F. Hoang, A. Engler, and M. F. Kaplon, Proc. International Conference on Mesons and Recently Discovered Particles, Padova-Venezia II- 48, 1957.
16. European K^--Stack Collaboration, Proc. International Conference on Mesons and Recently Discovered Particles, Padova-Venezia II-5, (1957).
17. Cork, Lambertson, Piccioni, and Wenzel, Phys. Rev. 106, 167 (1957).
18. W. H. Barkas, Proceedings of the Seventh Annual Rochester Conference, VIII - 30, 1957.
19. Bayard Rankin, Rev. Sci. Instr. 25, 675 (1954).

20. Walter H. Barkas, Nuovo cimento 8, 201 (1958).
21. Walter H. Barkas, Emulsion Statistics, UCRL-8687, March 1959.
22. Eisenberg, Koch, Lohrmann, Nikolic, Schneeberger and Winzeler, Nuovo cimento 9, 745 (1958).
23. M. L. T. Kannangara and G. S. Shrikantia, Phil. Mag. 44, 1091 (1953).
24. W. H. Barkas and D. M. Young, Emulsion Tables. I. Heavy-Particle Functions, UCRL-2579 (rev)., Sept. 1954.
25. G. Baroni and C. Castagnoli, Nuovo cimento 12, Suppl., 364 (1954).